Near-Infrared Light Photocontrolled Targeting, Bioimaging, and Chemotherapy with Caged Upconversion Nanoparticles *in Vitro* and *in Vivo*

Yi-Hsin Chien,[†] Yu-Lin Chou,[†] Shu-Wen Wang,[†] Shu-Ting Hung,[‡] Min-Chiau Liau,[‡] Yu-Jo Chao,[†] Chia-Hao Su,[‡,*] and Chen-Sheng Yeh[†,*]

[†]Department of Chemistry, Center for Micro/Nano Science and Technology, and Advanced Optoelectronic Technology Center, National Cheng Kung University, Tainan, 701 Taiwan and [‡]Center for Translational Research in Biomedical Sciences, Kaohsiung Chang Gung Memorial Hospital, Kaohsiung, 833 Taiwan

ABSTRACT The major challenge in current chemotherapy is to increase local effective therapeutic concentration of drugs as well as to minimize toxicity and side effects for patients. The targeted delivery of drugs to their desired site of action in a controlled manner plays an essential role in the development of drug formulations. A photocage refers to a caged molecule rendered biologically inert by a photolabile protecting group. Molecules are illuminated with light to liberate the caged group and then become active forms. In this study, we formulate upconversion nanoparticles (UCNPs) as the NIR-triggered targeting and drug delivery vehicles that successfully deliver *in vitro* and *in vivo* for near-infrared light photocontrolled targeting, bioimaging, and chemotherapy.

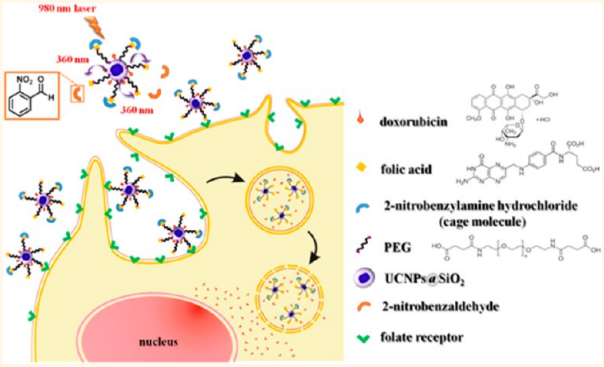

It is noted that there has been no report on the systemic administration UCNP-based drug delivery agents for evaluation of bioimaging and chemotherapy. To achieve phototargeting, the tumor-homing agent (*i.e.*, folic acid) has been constructed as a photoresponsive molecule. For the chemotherapeutic effect, the antitumor drug doxorubicin is thiolated on the surface of UCNPs, forming a disulfide bond that can be cleaved by lysosomal enzymes within the cells. The caged UNCPs can serve as a platform for the improvement of selective targeting and possible reduction of adverse side effects from chemotherapy.

KEYWORDS: drug delivery · upconversion nanoparticles · phototargeting · nanotechnology · chemotherapy

The major challenge in current chemotherapy is to increase local effective therapeutic concentration of drugs as well as to minimize toxicity and side effects for patients. Several strategies including (1) active targeting therapy, (2) sensitization of cancer cells to therapeutic modalities, and (3) localized controlled activation for release of drugs can be implemented to approach this goal. Active targeting provides an efficient delivery of drug to the malignant cells, resulting in high local concentration of chemotherapeutics. However, such an active targeting approach still suffers from certain limitations, such as the heterogeneity in receptor expression among different cancer cells. Thus, the targeted delivery of drugs to their desired site of action in a controlled manner plays an essential role in the development of drug formulations. It is fascinating to construct a stimuli-responsive active targeted drug delivery system. Recently, a phototargeting approach offering on-demand targeting capability has attracted increasing interests.[1−3] Phototargeting refers to a caged molecule rendered biologically inert by a photolabile protecting group. Molecules are illuminated with light to liberate the caged group and then become active forms. The phototargeting approach could be potentially adopted to improve specific adsorption and cellular uptake for cell-penetration peptides and tumor-homing agents. However, the use of high-energy

* Address correspondence to csyeh@mail.ncku.edu.tw, chiralsu@gmail.com.

Received for review May 13, 2013 and accepted September 26, 2013.

Published online September 26, 2013
10.1021/nn402399m

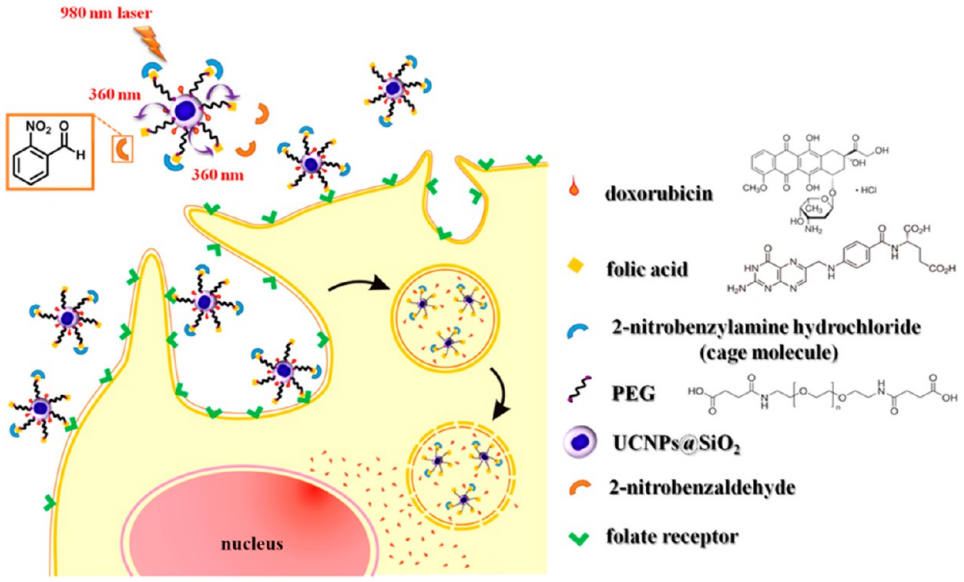

Scheme 1. Illustration of photocaged UCNPs following NIR laser activation to remove cage molecules and subsequent targeting of cancer cells.

ultraviolet (UV) light, which can hardly penetrate the tissue, hampers its potential use in further *in vivo* biomedical applications. One way to bypass this hurdle is to utilize near-infrared (NIR) responsive UCNPs. UCNPs are capable of converting NIR light into a range of different wavelengths of light in UV, visible, and NIR regions by emitting high-energy photons from lower-energy photons.[4−13] Herein, we report a lanthanide-doped upconverting nanoparticle (UCNP)-based drug agent that selectively delivers drug to the targeted area on the basis of a photocage technique that uses light to manipulate photoactive compounds.

It has been established that the UCNPs possess several advantages including weak background fluorescence that can enhance the signal-to-noise ratio, low photobleaching, and deep tissue penetration without causing photodamage.[14−16] Because of the aforementioned benefits, UCNPs have received significant attention and much efforts for *in vitro* and *in vivo* applications in biolabeling and optical fluorescence imaging.[9,17−28] Their studies for *in vivo* therapeutic treatments remain limited in some pioneering examples where the photodynamic therapy, by taking advantage of the energy conversion in UCNPs, has been a focus to date.[29−34] Meanwhile, there has been no report on the systemic administration of UCNP-based drug delivery agents for evaluation of bioimaging and chemotherapy. The limited progress with a handful of studies have been made to demonstrate *in vitro* drug storage/release behavior or intracellular delivery of drugs with UCNPs.[35−38] For example, the drugs were either encapsulated in the porous structure, such as core−shell UCNPs or the mesoporous SiO_2-coated UNCPs, or carried by physical adsorption on UCNPs.

In this study, we introduced UCNP as a NIR-triggered targeting and drug delivery vehicle. The UV photons emitted by the UCNPs triggered photoresponsive folic acid (FA) by activating the photocleavage reaction to proceed targeting of cancerous cells. FA is a low molecular weight vitamin and has high affinity to folate receptor (FR), a membrane-anchored protein.[39−41] FR can be found often overexpressed on cancer cell surfaces.[42−44] However, the number of FR expressed heterogeneously among different cancer cells limits the tumor delivery capacity of FR endocytosis. In addition, significant FR expression occurs in the normal kidney cells also.[45,46] In order to improve targeting selectivity, we have masked FA using a caging molecule and conjugated on UCNPs. Upon irradiation of a 980 nm diode laser on UCNPs, the emitted UV light (360 nm) photocleaved the *o*-nitrobenzyl (ONB) photolabile group, releasing cage molecules that allowed FA to target FR (Scheme 1). To provide chemotherapeutic function, doxorubicin (DOX) was thiolated on the surface of UCNPs, forming a disulfide bond that can be cleaved by lysosomal enzymes within the cells.[47−50]

RESULTS AND DISCUSSION

Synthesis and Characterization of UCNPs. The UCNPs, $NaYF_4$:Yb,Tm, were synthesized following the reported literature.[51,52] Figure 1a shows the TEM image of the dispersed and uniform size UCNPs with an average diameter of *ca.* 35 ± 2 nm. The visual photograph of UCNPs in hexane displayed a blue color (inset of Figure 1a). The high-resolution TEM (HR-TEM) image (Figure 1b) of a single UCNP showed hexagonal crystal structure with an interplanar distance of 2.7 Å corresponding to the (200) plane of the $NaYF_4$ nanocrystals. The electron diffraction measurements further supported single-crystalline structure (inset of Figure 1b). X-ray diffraction (XRD) patterns (Figure 1c) can be

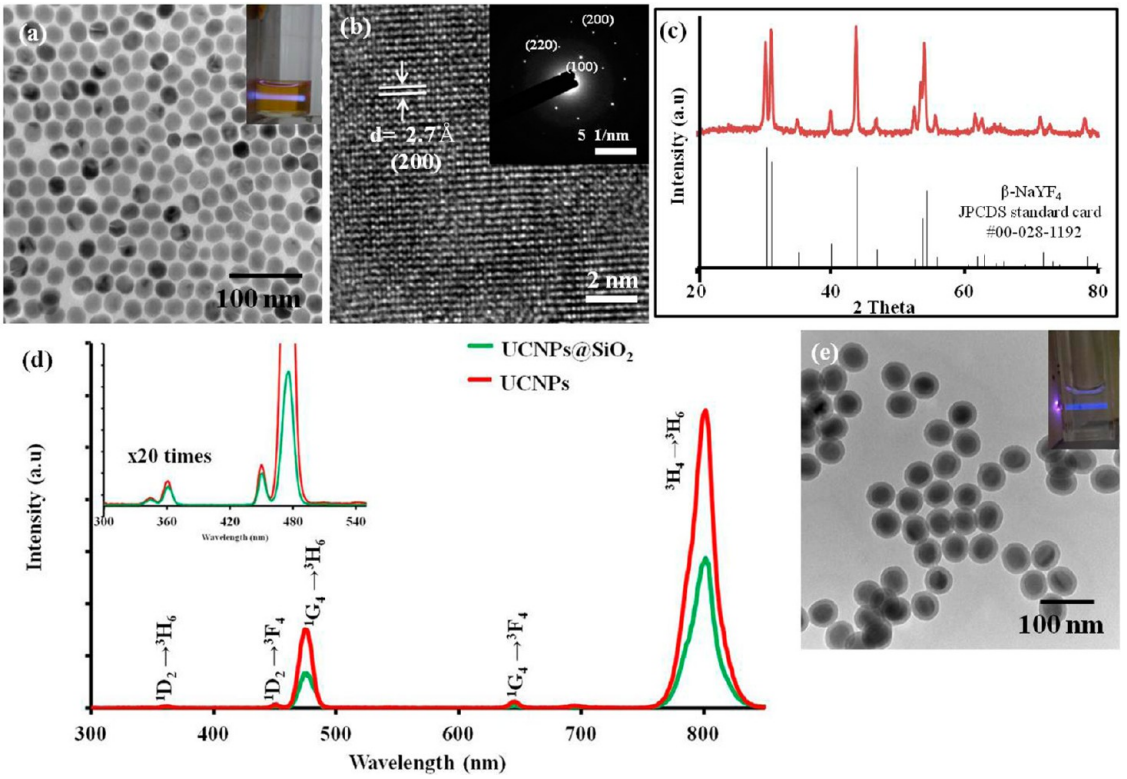

Figure 1. (a) TEM image of $NaYF_4$:Yb,Tm nanoparticles (inset: visual photograph in hexane), and the corresponding (b) HR-TEM image (inset: electron diffraction pattern) and (c) XRD pattern of $NaYF_4$:Yb,Tm nanoparticles. (d) Fluorescence spectra of $NaYF_4$:Yb,Tm nanoparticles in hexane and silica-coated $NaYF_4$:Yb,Tm particles in H_2O at a concentration of 0.2 mg/mL under 980 nm excitation. (e) TEM image of silica-coated $NaYF_4$:Yb,Tm nanoparticles (inset: visual photograph in H_2O).

indexed to pure hexagonal-phase $NaYF_4$ crystals (JCPDS standard card no. 28-1192). The as-prepared UCNPs were capped with oleic acid and hence dispersed in hexane. Under excitation of UCNPs in hexane at 980 nm diode laser, the fluorescence spectra (Figure 1d) showed emission peaks at 346, 360, 450, 474, 646, and 800 nm, which were assigned to the $^1I_6 \rightarrow {}^3F_4$, $^1D_2 \rightarrow {}^3H_6$, $^1D_2 \rightarrow {}^3F_4$, $^1G_4 \rightarrow {}^3H_6$, $^1G_4 \rightarrow {}^3F_4$, and $^3H_4 \rightarrow {}^3H_6$ transition from Tm^{3+}, respectively.[53,54]

For further biomedical studies, the as-prepared hydrophobic UCNPs were coated with a silica shell to become hydrophilic by following the reported microemulsion method.[55−58] The UCNPs@SiO_2 had a particle size of 49.8 nm, measured by TEM, with a homogeneous silica deposition of 7.4 ± 1.3 nm thickness (Figure 1e). UCNPs@SiO_2 dispersed in H_2O retained the same emission spectral behavior and exhibited visible photoluminescence under the excitation of a 980 nm laser (inset of Figure 1e). The visible and NIR emission intensity of the UCNPs@SiO_2 in water decreased by ~40−50% efficiency compared to that in hexane. However, the intensity of the UV peak at 360 nm was not affected after silica shell coating (Figure 1d). For the *in vitro* and *in vivo* studies, we have dispersed UCNP@SiO_2 in each of the following: cell culture Dulbecco's modified Eagle's medium (DMEM), phosphate buffered saline (PBS) with pH 7, and PBS with pH 5. PBS at pH 7 mimics the extracellular environment, whereas PBS at pH 5 is examined for the intracellular endosome/lysosome environment. UNCP@SiO_2 showed no aggregation and no degradation of the silica shell for 10 days (Supporting Information Figure S1). To form PEGylated UCNPs@SiO_2 with the anticancer drug DOX conjugated on the surface, UCNPs@SiO_2 were further modified with 3-aminopropyltriethoxysilane (APTES). The change in zeta-potential from −25.9 mV for UCNPs@SiO_2 to +33.0 mV for UCNPs@SiO_2-APTES confirmed the proper loading of APTES on the surface of UCNPs@SiO_2, which exposes the $-NH_2$ group for further anchoring. There was no change in the emission spectrum of modified UCNPs (UCNPs@SiO_2-APTES) as compared to UCNPs@SiO_2. It is noted that UCNPs@SiO_2-APTES can be stored over 3 months without any change in morphology and emission behavior. FTIR analysis gives information on the surface moiety and provides additional evidence about the transformation of particles from UCNPs with oleic acid to UCNPs with a silica layer, then to APTES-functionalized UCNPs@SiO_2 (Figure S2).

Next, we conjugated DOX and PEG (HOOC-PEG-COOH, MW = 6000) on UCNPs@SiO_2-APTES in sequence. The UCNPs@SiO_2-APTES containing amino groups were functionalized with *N*-succinimidyl 3-(2-pyridyldithio)-propionate (SPDP), which contains a disulfide bond in the spacer arms and can be cleaved by the reduction process with dithiothreitol (DTT). The detailed illustration

of surface modification can be seen in experimental section of Supporting Information. As a result of this cleavage, pyridine-2-thione (P2T) was released, which can be quantified at 343 nm absorbance, hence we are able to quantify the number of SPDP molecules on the UCNP surface, giving 2/3 amino groups on the UCNPs@SiO_2-APTES modified with SPDP molecules (Figure S3). The remaining amino groups were then conjugated with carboxylate groups of PEG molecules (MW 6000) to form an amide bond through (1-ethyl-3-(3-dimethylaminopropyl)carbodiimidehydrochloride and *n*-hydroxysuccinimide (EDC/NHS) chemistry. Dynamic light scattering (DLS) measurements showed average diameter of 116 nm for the PEGylated UCNPs@SiO_2 particles. Once we formulated the PEGylated UCNPs@SiO_2, the DOX was incorporated on the surface, yielding PEGylated UCNPs@SiO_2-DOX. DOX thiolation is in accordance with the reported method where the 2-iminothiolane hydrochloride was added to react with DOX.[59] Subsequently, the thiolated DOX was conjugated to SPDP molecules on the particle surface. Once again, the cleavage of disulfide bonds by the reduction of DTT was used to quantify 0.024 mol of DOX per mole of Y^{3+} ion on the PEGylated UCNPs@SiO_2. The quantity of DOX was measured from fluorescence emission at 555 nm of the liberated DOX in the supernatant solution after reaction and calculated based on the calibration curve according to DOX concentration.

Prior to conjugation of FA on PEGylated UCNPs@SiO_2, we examined caging effectiveness in pure FA without particles. The carboxylate moiety of FA exhibits high affinity toward the folate receptor of the cell surface.[60] ^{1}H NMR spectroscopy of free FA displayed the appearance of a peak at 12.8 ppm, indicating the presence of carboxylate groups (Figure S4a). Once the −COOH groups of FA were completely masked by the molecule 2-nitrobenzylamine (NBA) through formation of amide bonds by EDC/NHS conjugation, the peak at 12.8 ppm disappeared accompanied with multiplet peaks in the range of 7−8.5 ppm chemical shift, attributed to aromatic rings of NBA (Figure S4b). FA/NBA mole ratio (adding amount ratio) is 1/5.

The aforementioned results successfully demonstrated that −COOH groups of FA can be caged using photolabile protecting NBA molecules. The caged folate design was then applied on the PEGylated UCNPs@SiO_2 where the exposed −COOH groups of PEG formed an amide bond with the $-NH_2$ groups of the opposite terminus of FA. For the purpose of simplicity, the PEGylated UCNPs@SiO_2 particles, used to evaluate the conjugation of FA and cage NBA, did not carry DOX for the following experiments. The proper FA functionalization was confirmed by the appearance of the FA absorption band at 284 and 360 nm from UV−vis spectra (Figure S5). The amount of immobilized FA was measured from the decrease in the UV−vis absorbance intensity of FA left in the supernatants and calculated based on a calibration curve according to FA concentration. It was estimated that there was approximately 0.015 mol FA/mol Y^{3+} ions for PEGylated UCNPs@SiO_2. The zeta-potential measurements revealed the surface charges as −26.6 mV on folate-PEGylated UCNPs@SiO_2. Additional evidence of FA conjugation was obtained from FTIR spectra of the corresponding molecules (Figure S6). The absorption peaks can be fitted with pure FA molecules. Subsequently, the folate-PEGylated UCNPs@SiO_2 was further conjugated with cage NBA. The conjugation amount was calculated as 0.011 mol NBA/mol Y^{3+}. Because of the similarity in aromatic characteristics between cage NBA and FA, both UV−vis and FTIR measurements cannot give clear evidence for the presence of NBA caging on folate-PEGylated UCNPs@SiO_2. The photolabile nature of the cage NBA was evidenced by the observation of the absorbance peak of the photocleavage product 2-nitrobenzaldehyde appearing at 285 nm. Photolysis was performed using a Hg lamp with a distance fixed at 3 cm between the optical fiber head and the illuminating place. The caged folate-PEGylated UCNPs@SiO_2 was dispersed in PBS buffer (pH 7.4) and exposed to light as a function of illumination time (Figure S7). The 2-nitrobenzaldehyde increases as exposure time is prolonged. In addition, the reverse-phase HPLC performance was conducted to observe cleavable 2-nitrobenzaldehyde product by irradiation of caged folate-PEGylated UCNPs@SiO_2, as well. A 980 nm laser irradiation detached the 2-nitrobenzaldehyde with absorption at 285 nm, which was observed at a retention time of 19.4 min in HPLC measurement (Figure S8).

***In Vitro* Phototargeting Studies.** We have chosen malignant HeLa human cervical epithelial carcinoma cells (FR-positive), A549 human lung adenocarcinoma epithelial cells (FR-negative), and MRC-5 normal human fibroblast cells to inspect expression of folate receptors. The cell binding assays were evaluated using FOLR1 monoclonal antibody and secondary antibodies (NorthernLights antimouse IgG-NL493) (Figure S9). The fluorescent immunocytochemistry (ICC) staining results showed that the HeLa cells displayed stronger FITC fluorescence, indicating greater expression of folate receptors on the HeLa cell membrane, whereas A549 and normal MAC-5 cells showed no apparent FITC fluorescence. For the validation of antimouse IgG-NL493 with human cells, we also used incubation buffer without primary antibody (human FOLR 1) to characterize the nonspecific binding of antimouse IgG-NL493 in HeLa cells (Figure S10). The secondary antibody of antimouse IgG-NL493 cannot bind on cell membranes with a folate receptor, and the fluorescence signal was not observed in this negative control. Following this fluorescent ICC examination, we compared the targeting performance of the caged folate-PEGylated UCNPs@SiO_2 bound to the cell surfaces of

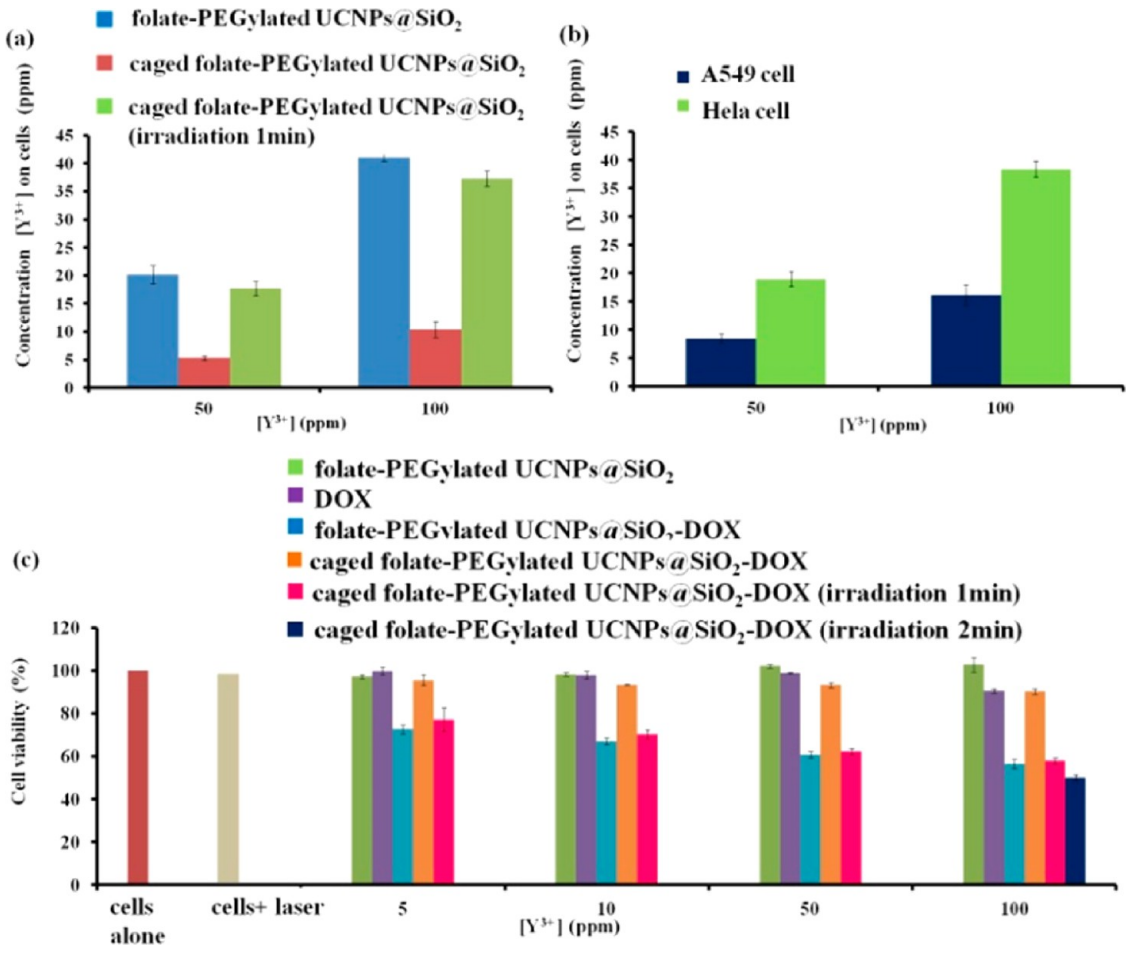

Figure 2. (a) Cell targeting of folate-PEGylated UCNPs@SiO_2 and caged folate-PEGylated UCNPs@SiO_2 particles for HeLa (FR-positive) cells at 4 °C for 20 min. The group exposed to light was performed using a 980 nm diode laser for 1 min irradiation at 11 W/cm^2. (b) Phototargeting studies of caged folate-PEGylated UCNPs@SiO_2 for HeLa (FR-positive) and A549 (FR-negative cells) cells at 4 °C upon 1 min laser irradiation (11 W/cm^2). (c) Cell viability studies of HeLa cells incubated individually with folate-PEGylated UCNPs@SiO_2, free DOX, folate-PEGylated UCNPs@SiO_2-DOX, and caged folate-PEGylated UCNPs@SiO_2-DOX with a series of dosage (5, 10, 50, 100 ppm) based on Y^{3+} concentration. The 5, 10, 50, and 100 ppm correspond to 0.13, 0.27, 1.34, and 2.67 μM of DOX carried by the particles. One minute of irradiation was operated under 11 W/cm^2, while 2 min irradiation was conducted at 9.6 W/cm^2.

HeLa and A549 cells at 4 °C, which is a temperature known to retard vesicular trafficking pathways.[61,62] Prior to perform phototargeting studies of caged folate-PEGylated UCNPs@SiO_2 using a 980 nm diode laser, the 980 nm irradiation of H_2O was performed as a function of exposure time under different laser power intensity. Because H_2O has an absorbance at 980 nm, the elevation of H_2O temperature depended on the laser intensity and irradiation time (Figure S11). We have chosen conditions of 11 W/cm^2 and 1 min exposure for irradiation, which resulted in 37.7 °C to avoid overheating and damaging cancer cells. As expected, the uncaged folate-PEGylated UCNPs@SiO_2 readily attached on HeLa cells following a process with 20 min incubation at 4 °C (Figure 2a).

The untargeting nanoparticles were removed by PBS wash and then subjected to inductively coupled plasma atomic emission measurements for the particle uptake. The uptake increased with particle dosage. On the contrary, caged folate-PEGylated UCNPs@SiO_2 showed significantly reduced affinity to folate receptor with only some particle uptake. Because 70% of FA was blocked by NBA as determined from aforementioned results, the residual unmasked FA could have shown meager binding activity resulting in some particles on cells when treated with caged folate-PEGylated UCNPs@SiO_2. Upon 980 nm laser irradiation for 1 min at 11 W/cm^2, the number of particles uptaken by cells apparently increased (Figure 2a), where the cells were exposed to NIR light for 1 min, followed by additional 20 min incubation performed at 4 °C. The control experiments using PEGylated UCNPs@SiO_2 without FA were conducted to evaluate cellular uptake, as well (Figure S12). No apparent particles uptaken by cells were seen without laser irradiation. In the absence of laser irradiation, the cells treated with PEGylated UCNPs@SiO_2 were subjected to incubation at 4 °C for 20 min before evaluation. Phototargeting experiments were also carried out on malignant lung A549 cells to compare with those of HeLa cells; the low FR

expression of A549 exhibited much less particle uptake (Figure 2b). These results support the susceptibility of our phototargeting design to improve selective uptake for tumor-homing agents.

Intracellular Drug Delivery Studies. Next, the intracellular drug delivery was studied for caged folate-PEGylated UCNPs@SiO_2 carrying DOX (caged folate-PEGylated UCNPs@SiO_2-DOX) (Figure 2c). TEM image shows caged folate-PEGylated UCNPs@SiO_2-DOX retaining dispersion without aggregation even after 3 months storage (Figure S13). As shown in Figure 2c, there are materials of folate-PEGylated UCNPs@SiO_2, free DOX, folate-PEGylated UCNPs@SiO_2-DOX, and caged folate-PEGylated UCNPs@SiO_2-DOX individually treated with HeLa cells and subjected to MTT assays. The particles treated with HeLa cells had the dosages of 5, 10, 50, and 100 ppm that were based on Y^{3+} concentration corresponding to 0.13, 0.27, 1.34, and 2.67 μM of DOX carried by UCNPs, respectively. To demonstrate the on-demand drug toxicity only when the luminescent light was on, all of the experiments followed the same sequence with 4 °C/20 min incubation → 37 °C/24 h culture, so that the particles bound to the cell surface at 4 °C was internalized into cells at 37 °C. The untargeted particles were washed away by PBS before 24 h of culture at 37 °C. For the groups with light exposure, the HeLa cells treated with caged folate-PEGylated UCNPs@SiO_2-DOX were irradiated for 1 (11 W/cm^2) or 2 min (9.6 W/cm^2) at 4 °C and then incubated for 20 min at 4 °C prior to 24 h culture. No cell reduction was observed when cells alone were exposed to NIR laser. The material, folate-PEGylated UCNPs@SiO_2, did not show toxicity when the dosage was up to 100 ppm. The free DOX also did not cause noticeable cell toxicity, as the viability remains above 90%. On the other hand, folate-PEGylated UCNPs@SiO_2-DOX particles exhibited their targeting potential for FR-positive HeLa cancer cells.

The reduction in cell viability increased with DOX drug concentration. The cell viability dropped to 57% at 2.67 μM of DOX (100 ppm [Y^{3+}]). When the folate was caged, caged folate-PEGylated UCNPs@SiO_2-DOX, the targeting ability was reduced, and hence MTT evaluation displayed an increase in cell survival rate at different particle dosage, where the survival value was up to 90% at 2.67 μM DOX (100 ppm [Y^{3+}]). Upon 980 nm laser (11 W/cm^2) irradiation for 1 min, the group of caged folate-PEGylated UCNPs@SiO_2-DOX apparently increased cell damage and reduced viability to ~57% at 2.67 μM DOX (100 ppm [Y^{3+}]). Basically, the caged folate-PEGylated UCNPs@SiO_2-DOX (with laser irradiation) exerted an effect on cell damage comparable to those of folate-PEGylated UCNPs@SiO_2-DOX. It is noted that the degree of the cell viability is associated with both factors of laser intensity and irradiation period. For example, ~50% survival rate was obtained when the cells were treated with particles exposed to the 980 nm diode laser with 9.6 W/cm^2 for 2 min. We further visualized subcellular localization of the DOX and particle uptake. Folate-PEGylated UCNPs@SiO_2-DOX and caged folate-PEGylated UCNPs@SiO_2-DOX were incubated with HeLa cells following the sequence with 4 °C/20 min incubation → 37 °C/24 h culture. The differential interference contrast (DIC) and confocal fluorescence field images are illustrated in Figure S14. The lysosomes were stained with LysoTracker (green color). The red signal represented DOX. We found some DOX (red color) were packaged with lysosomes (green color) as the intracellular delivery pathway. In terms of release, a large quantity of DOX was distributed across the cytoplasm and was not colocalized with lysosome tracker, as well. This suggests that DOX located in the cytosol and may have escaped from the lysosomes to the cytosol. No red fluorescence was seen from the cells treated with caged folate-PEGylated UCNPs@SiO_2-DOX (in the absence of a 980 nm laser illumination), indicating that UCNPs cannot effectively enter into cells due the lack of FA targeting ability.

***In Vitro* Cell Imaging.** The NIR light-triggered FA-targeting and intracellular drug delivery was further demonstrated for *in vitro* cell images. Figure 3 shows confocal fluorescence field images of cells alone (Figure 3a), uncaged (Figure 3b), caged (Figure 3c), and laser-treated (Figure 3d) caged folate-PEGylated UCNPs@SiO_2-DOX particles treated with HeLa cancer cells. The images used a modified laser-scanning confocal fluorescence microscope equipped with an external 980 nm laser as the excitation source to detect an upconversion signal (emission 800 nm, shown as purple color) from UCNPs. Figure 3a displays cells alone without treatment of UCNPs. As shown in Figure 3b for folate-PEGylated UCNPs@SiO_2-DOX, the fluorescence spots of upconversion signals appeared in HeLa cells, indicating the distribution of folate-PEGylated UCNPs@SiO_2-DOX particles across the cytoplasm. At 24 h, the DOX (red color) was released in the cytoplasm and entered into the nuclei, resulting in cell shrinkage due to the cytotoxicity of cancer cells. Figure 3c shows the cells treated with caged folate-PEGylated UCNPs@SiO_2-DOX without laser irradiation, where cells retained intact morphology and revealed some particle uptake with dim fluorescence. In this case, we barely observed red fluorescence of DOX. Meanwhile, when the caged folate-PEGylated UCNPs@SiO_2-DOX received the NIR laser, the obvious bright fluorescence (shown as purple color) was seen from HeLa cells (Figure 3d). The nuclei and cytoplasms of cancer cells shrank, indicating cytoplasm destruction and nuclei damage.

***In Vivo* Photoluminescence Imaging and Therapeutic Efficacy.** Prior to the investigation of the feasibility of the current phototargeting approach, the folate-PEGylated UCNPs@SiO_2 was intratumorally injected to examine the effectiveness in NIR luminescence (emission 800 nm).

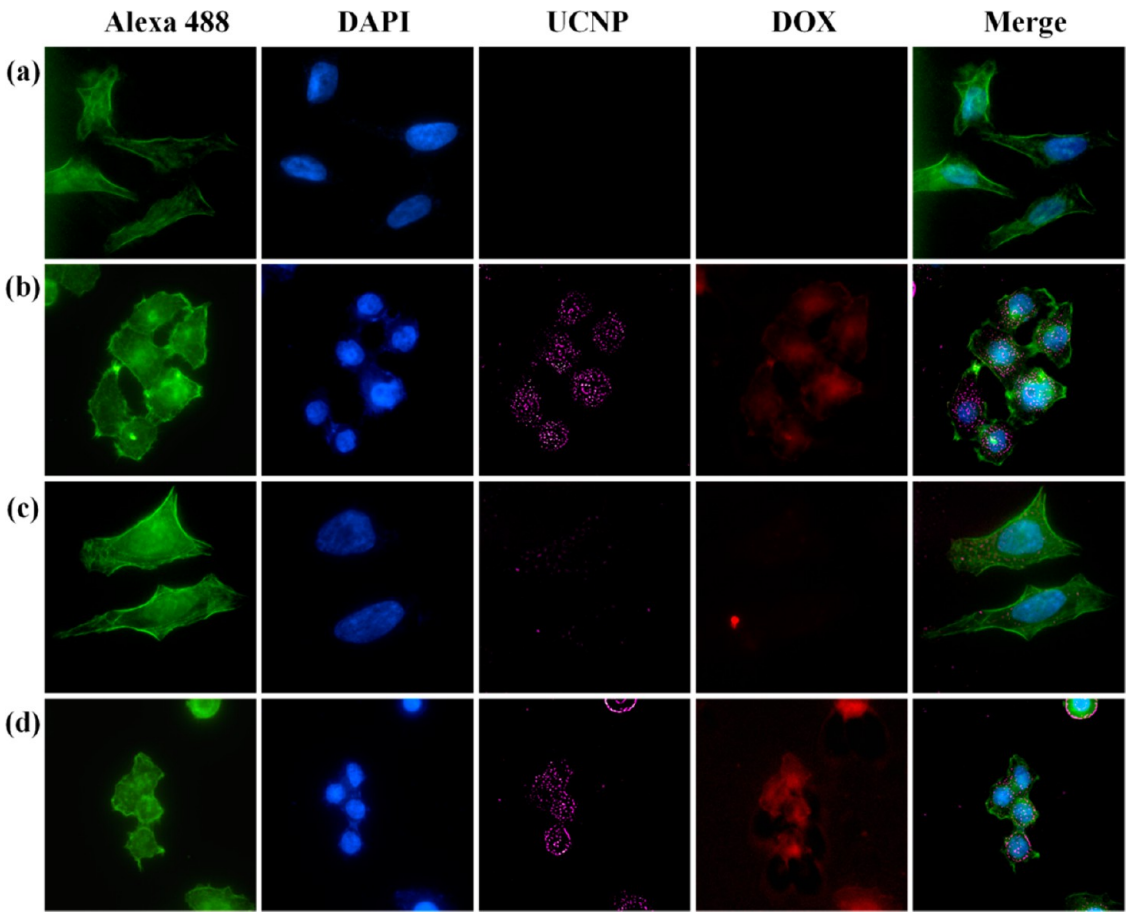

Figure 3. Confocal images of HeLa cells incubated with (a) cells alone, (b) folate-PEGylated UCNPs@SiO_2-DOX, (c) caged folate-PEGylated UCNPs@SiO_2-DOX, and (d) caged folate-PEGylated UCNPs@SiO_2-DOX by exposure of a 980 nm diode laser (9.6 W/cm^2) for 2 min at 4 °C. All of the experiments followed the sequence with 4 °C/20 min incubation → 37 °C/24 h culture. After 20 min incubation at 4 °C, the untargeted nanoparticles were removed by PBS wash. The cell cytoskeleton was stained with Alexa 488 phalloidin (green). The nuclei were stained with DAPI. The merged image represents Alexa 488 + DAPI + UCNP emission.

The apparent NIR emission of the upconverting NPs can be detected on the HeLa tumor site upon 980 nm laser irradiation (Figure S15). The evaluation of *in vivo* photoluminescence imaging and therapeutic efficacy was performed by injection of UNCPs through tail vein into mice bearing HeLa tumors. Figure 4a shows targeted upconversion NIR luminescence imaging of tumors. For the laser-treated group, the caged folate-PEGylated UCNPs@SiO_2-DOX (2 mg DOX/kg) were injected through intravenous injection, and then the 980 nm diode laser (1.8 W/cm^2) was turned on to irradiate the tumor region for 1 h. The upconversion NIR emission was then monitored over time (post-particle injection) in the tumor. For those time-dependent NIR images, except the second image (post-1 h) for the laser-treated group taken upon 1 h irradiation as described above, the 980 nm laser was turned on less than 1 min for observation of upconversion NIR luminescence. The emitted NIR light from UCNPs was clearly observed for the mice with laser-treated caged folate-PEGylated UCNPs@SiO_2-DOX. The brightest NIR emission was observed at post-5 h, and then the fluorescence diminished at post-24 h (Figure 4b). In a marked contrast, the mice treated with caged folate-PEGylated UCNPs@SiO_2-DOX without exposure of 1 h laser exhibited dimmed emission. This provides strong evidence in effectively enhanced upconversion NIR fluorescence due to NIR-triggered uncaging with an increase of UNCP uptake by the tumor. The mice administered with PBS solution showed no NIR emission in the tumor region. We further performed *ex vivo* imaging analysis of DOX fluorescence (emission 580 nm) at the time points of post-1, 5, and 24 h (Figure 4c). The appearance of red fluorescence of DOX is consistent with the upconversion NIR fluorescence. The maximum fluorescence of the tumor was reached at post-5 h. The signal was retained even at 24 h, although the intensity dropped to some extent. This might reflect that DOX was cleaved from UNCPs left in tumor cells, while the clearance of UCNPs from the tumor led to the loss of NIR fluorescence, as seen in Figure 4a. Finally, we evaluated the efficacy of the caged folate-PEGylated UCNPs@SiO_2-DOX particle as an *in vivo* chemotherapeutic agent. The tumor growth was monitored in terms of tumor volume changes (Figure 4d).

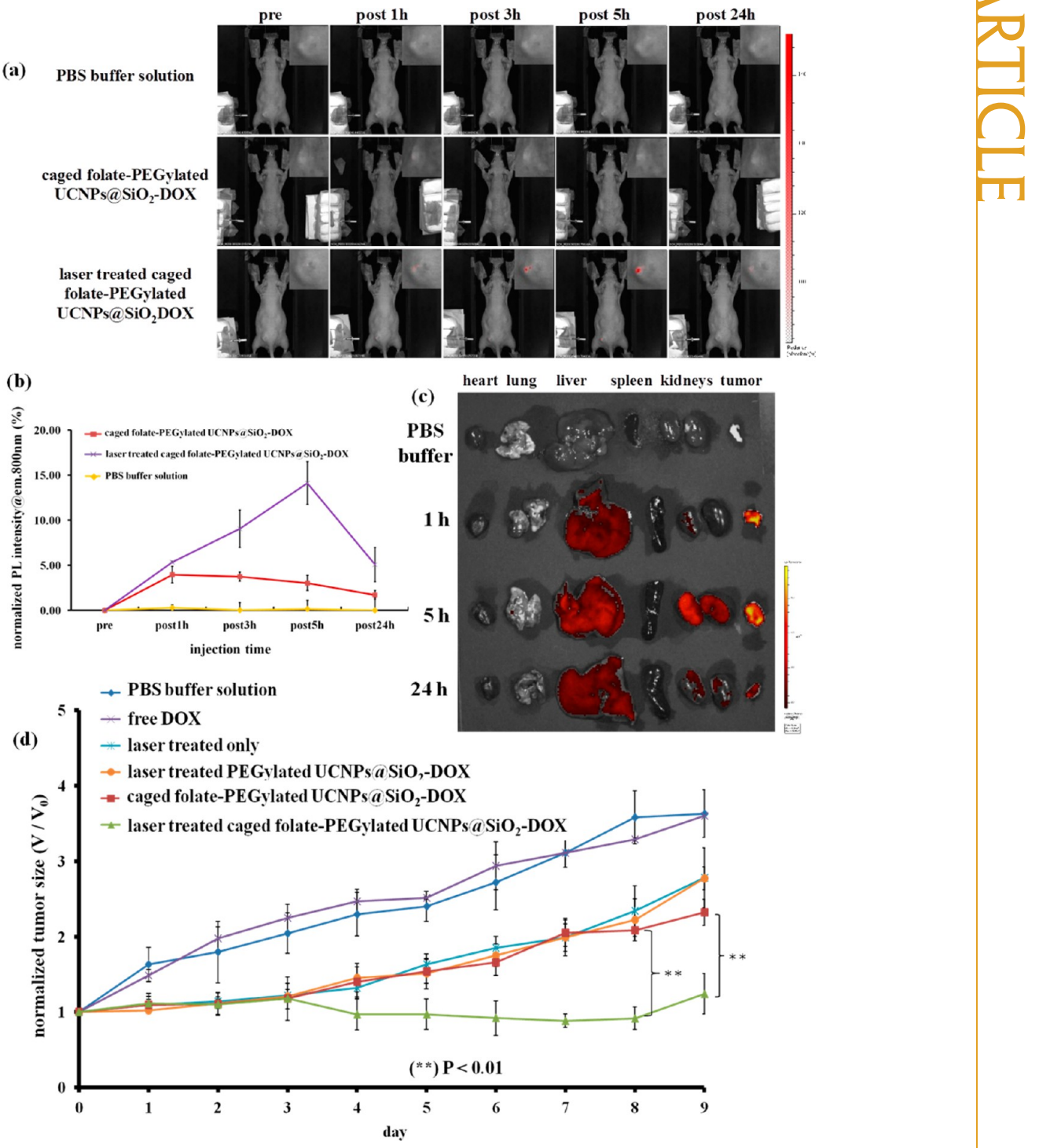

Figure 4. (a) Time course upconversion NIR luminescence (emission 800 nm) images of caged folate-PEGylated UCNPs@SiO_2-DOX nanoparticles without NIR laser irradiation. Insets show the enlarged tumor region. (b) NIR luminescence intensity of the tumor region at various post-injection time corresponds to the groups shown in (a). The intensity ratio (%) was calculated relative to the preinjection. Error bars are based on five mice per group ($n = 5$). (c) *Ex vivo* DOX fluorescence (emission 580 nm) images of the dissected organs and tumor from the group of laser-treated caged folate-PEGylated UCNPs@SiO_2-DOX nanoparticles of (a). (d) Tumor growth suppression monitored in terms of tumor volume changes. Error bars are based on five mice per group ($n = 5$). **$P < 0.01$ calculated and compared to caged folate-PEGylated UCNPs@SiO_2-DOX (without laser irradiation).

The xenografted mouse tumor model was established by subdermal injection of HeLa cancer cells. Thirty nude mice bearing HeLa tumors were divided into six groups including control (PBS received), free DOX, laser only, caged folate-PEGylated UCNPs@SiO_2-DOX, PEGylated UCNPs@SiO_2-DOX + laser, and caged folate-PEGylated UCNPs@SiO_2-DOX + laser. The mice bearing tumors (~92 mm^3) were injected with caged folate-PEGylated UCNPs@SiO_2-DOX with a dosage of 2 mg DOX/kg through tail vein injection. Tumors were

exposed to 980 nm (1.8 W/cm^2) laser for 1 h after particles were injected into mice for the groups of PEGylated UCNPs@SiO_2-DOX + laser and caged folate-PEGylated UCNPs@SiO_2-DOX + laser. The group treated with free DOX received intravenous injection with the same amount (2 mg DOX/kg) of DOX carried by UNCPs. The groups with laser only, PEGylated UCNPs@SiO_2-DOX + laser, and caged folate-PEGylated UCNPs@SiO_2-DOX + laser displayed a trend with delay change in tumor size at the initial 3 days. Considering H_2O absorbance at 980 nm wavelength, the *in vivo* temperatures were monitored in 1 h using a thermocouple needle when a 980 nm diode laser irradiated the tumor site. The surface temperature of the skin at the irradiated tumor was measured as 37−38 °C after 1 h irradiation. The temperature at 3 mm depth beneath the irradiated tumor skin was mildly increased to 41−42 °C, a temperature to avoid vascular collapse,[63,64] at the beginning 20 min, and then became constant at the end of the 1 h period of irradiation. The lower temperature at the tumor surface is presumably due to convective cooling at the surface. Thermographic analysis of tumor temperature using a Thermo Tracer H2640 (NEC, Japan) camera was also performed and indicated a maximum temperature of ~39 °C in the region of the irradiated tumor after 1 h illumination (Figure S16). Continuing to monitor tumor change revealed that the tumors from the group with caged folate-PEGylated UCNPs@SiO_2-DOX + laser apparently dropped on day 4, whereas the tumors of other groups grew as days prolonged. The group that received caged folate-PEGylated UCNPs@SiO_2-DOX with subsequent laser exposure showed an effective antitumor effect. The tumor growth was significantly inhibited to some extent, although it continually existed post-treatment and displayed a much slower growth rate compared to the other control groups ($P < 0.01$ at 8 and 9 days compared to the caged folate-PEGylated UCNPs@SiO_2-DOX treated group without laser). P value is 0.062 at 9 day between the groups with laser only and PBS, showing no statistically significant difference. The tumors were not completely regressed in our pilot study. Further optimization of the UCNP design may warrant more promising results to exploit the phototargeting strategy *in vivo*. For example, improvement in UV emission intensity may be possible by doping of Gd ions in the synthesis of UCNPs, which is underway. Stronger UV intensity might facilitate enhancement of the uncaging process.

CONCLUSION

The on-demand targeting incorporation with photomodulation is a fascinating approach. We present this proof of concept that can be successfully applied to nanoparticles using UCNPs as the NIR-triggered targeting vehicles. Upon irradiation of a 980 nm diode laser, the emitted UV light uncaged a photolabile group and allowed folate-conjugated UNCPs to target cancer cells. Our evidence of *in vitro* and *in vivo* imaging and chemotherapeutic efficacy supported the idea that the caged UNCPs can serve as a platform for the improvement of selective targeting and reduction of adverse side effects from chemotherapy.

MATERIALS AND METHODS

Materials. Anhydrous YCl_3 (99.99%), $YbCl_3$ (99.9%), $TmCl_3$ (99.9%), NH_4F (≥99.9%), 1-octadecene (90%), oleic acid (90%), IGEPAL CO-520, *O*,*O*′-bis[2-(succinylamino)ethyl]polyethylene glycol (HOOC-PEG-COOH, MW 6000), 2-nitrobenzylamine hydrochloride (NBA), and *N*-hydroxysulfosuccinimide sodium salt (sulfo-NHS) (≥98.5%) were purchased from Aldrich Chemical Co. Tetraethyl orthosilicate (TEOS, 98%) and (3-aminopropyl)-triethoxysilane (APTES, 99%) were purchased from Acros. Folic acid (97%), 2-iminothiolane hydrochloride (≥98%), 3-(2-pyridyldithio)propionic acid *N*-hydroxysuccinimide ester (SPDP) (≥95%), *N*-(3-dimethylaminopropyl)-*N*′-ethylcarbodiimide hydrochloride (EDC), and doxorubicin hydrochloride (≥98%) were bought from Sigma-Aldrich. Sodium hydroxide (NaOH, 99%) and ethanol (99.9%) were obtained from Fullin.

Instrumentation. SDL-980-LM-5000T diode laser (Shanghai Dream Lasers Technology Co.) was utilized in the experiments. The size and shape of the nanoparticles were characterized by a Hitachi H-7500 transmission electron microscope operated at an acceleration voltage of 200 kV. The UV−vis absorbance intensity was measured using a UV−vis absorption spectrometer (Hewlett-Packard model 8453). Zeta-potential measurements were performed on a Zetasizer 3000HS-Advanced instrument at room temperature. An X-ray diffractometer (Shimadzu XRD-7000S (λ = 1.54060 Å, 30 kV, 30 mA)) was used to collect the XRD data. A FTIR (JASCO 200E FTIR) was used to measure the FTIR spectrum of prepared nanoparticles. Photoluminescence of $NaYF_4$:Yb^{3+},Er^{3+} (UNCPs) was obtained using a Fluoromax-4 spectrofluorometer (Horiba Scientific) equipped with a 980 nm laser excitation. The targeted UCNPs in cell images were captured using a confocal laser scanning microscope (ECLIPSE Ti series, NIKON) equipped with NIR980 nm diode laser. The Y^{3+} concentration (μg/mL) of UCNPs was determined by ICP-AES (Jobin Yvon JY138 spectroanalzer). The quantification of cell viability was done using an ELISA plate reader (Thermo Scientific Multiskan EX).

Synthesis of Caged Folate for NMR Characterization. Folic acid (FA) solution (100 μL, 1 mM in DMSO) and 2-nitrobenzenemethanamine (100 μL, NBA) hydrochloride (5 mM) were added into 1 mL of deionized water, followed by addition of 50 μL of 1-ethyl-3-(3-dimethylaminopropyl)carbodiimide hydrochloride (EDC, 1 mM) and 50 μL of *n*-hydroxysuccinimide (NHS, 1 mM) to react for 2 h at room temperature. The caged folate was purified by a silica-packing column. First, deionized water was added into the column to remove excess caging molecule, and then the NaOH solution (pH 8) was added into the column to collect solution. The precipitate was collected by the addition of aqueous HCl (pH <6) kept at room temperature for 1 h. Subsequently, the solution was centrifuged at 14 000 rpm for 5 min, and the supernatant was removed. The precipitates (caged folate) were dissolved in DMSO.

Synthesis of $NaYF_4$:Yb,Tm Nanoparticles (UCNPs). All reagents were of the highest research grade available. $NaYF_4$:Yb(24.7%),Tm (0.3%) nanoparticles were synthesized following a protocol reported previously.[51] In a typical procedure for the synthesis of $NaYF_4$:Yb/Tm, YCl_3(0.75 mmol), $YbCl_3$(0.247 mmol), and

$TmCl_3$(0.003 mmol) were dissolved in 2 mL of deionized water then mixed with 6 mL of oleic acid and 15 mL of 1-octadecene into a 100 mL flask. The solution was heated to 100 °C for 10 min (2 °C/min) and degassed at 156 °C for 30 min and then cooled to room temperature. A solution of 0.1482 g of NH_4F (4 mmol) and 0.1 g of NaOH (2.5 mmol) in 10 mL of methanol was added, and then the solution was kept at 50 °C for 30 min. Methanol was evaporated completely after heating at 75 °C for 30 min, and then the solution was heated to 300 °C for 1.5 h under argon atmosphere. Subsequently, the solution was cooled to room temperature. The UCNPs were precipitated from solution by adding acetone and then washed with hexane/ethanol and collected by centrifugation and redispersed in hexane.

Surface Modification Process

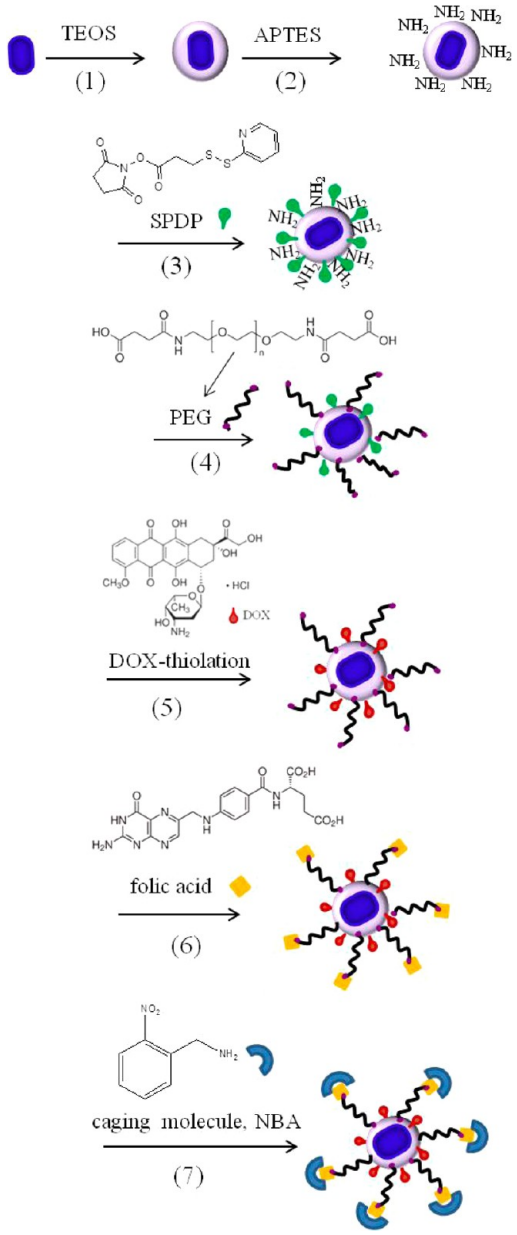

(1). Synthesis of Silica-Coated UCNPs. Water-soluble UCNPs were prepared according to the reported method.[52] The UNCPs (1200 ppm, 4 mL) in hexane (6 mL) were mixed with IGEPAL CO-520 (100 μL) and stirred for 10 min. Then, the transparent emulsion was formed by the addition of IGEPAL CO-520 (400 μL) slowly. The solution was mixed with aqueous ammonia (80 μL, 33%) and sonicated for 20 min. Further, 45 μL of tetraethyl orthosilicate (TEOS) was added into the solution and incubated for 16 h with vigorous stirring. UCNPs@SiO_2 were precipitated by adding acetone, and particles were collected by centrifugation at 13 000 rpm for 20 min and washed with 50/50 ethanol/water to store in ethanol.

(2). UCNPs@SiO_2-APTES Nanoparticles. To introduce amino groups ($-NH_2$) on the UCNPs@SiO_2 surface, the UCNPs@SiO_2 (3000 ppm) in 5 mL of ethanol were mixed with 100 μL of (3-aminopropyl)triethoxysilane (APTES) and stirred for 18 h. After 18 h, the nanoparticles were obtained through centrifugation at 14 000 rpm for 20 min and washed with ethanol to store in ethanol.

(3). UCNPs@SiO_2-APTES Conjugated with SPDP. The solution containing UCNPs@SiO_2-APTES (200 ppm) and *N*-succinimidyl-3-(2-pyridyldithiol)propionate (SPDP) reacted for 4 h. The amount of immobilized SPDP was measured from the UV−vis absorbance intensity of pyridine-2-thione (P2T), the product from SPDP reacted with dithiothreitol (DTT). Calculated based on a calibration curve according to the absorption band of P2T at 343 nm, we estimate that a maximum number of approximately 0.17 mol SPDP is attached per mole of Y^{3+} by adding 20 mM SPDP. Here, we took 3 mM SPDP concentration to immobilize the particles (about 2/3 amino groups covered on UCNPs); there are 122.3 mmol SPDP per mole of Y^{3+}.

(4). UCNPs@SiO_2-APTE Conjugated with PEG (PEGylated UNCPS@SiO_2). The residual amino groups of APTES molecules were modified with PEG (*O*,*O*′-bis[2-(succinylamino)ethyl]polyethylene glycol, MW 6000) to form amide bonds through 1-ethyl-3-(3-dimethylaminopropyl)carbodiimide hydrochloride/*N*-hydroxysuccinimide (EDC/NHS) chemistry. The UCNPs@SiO_2−SPDP (200 ppm) solution was mixed with 100 μL of PEG (4 mg/mL), EDC (10 mM, 100 μL), and NHS (10 mM, 100 μL). After 4 h, the solution was centrifuged at 14 000 rpm for 20 min, and the precipitates were washed three times with deionized water to remove excess PEG. The precipitates (PEGylated UCNPs@SiO_2) were dissolved in H_2O.

(5). Doxorubicin Hydrochloride (DOX) Thiolation on PEGylated UCNPs@SiO_2 (PEGylated UCNPs@SiO_2-DOX). DOX thiolation was followed according to the reported method.[59] 2-Iminothiolane hydrochloride (2-IT, 1 mM, 250 μL) and DOX (0.5 mM, 300 μL) were mixed at room temperature for 20 min. As-prepared PEGylated UCNPs@SiO_2 (200 ppm) were incubated with thiolated DOX solution for 3 h. The solution was centrifuged at 14 000 rpm for 20 min, and the precipitates were washed three times with DDW to remove excess DOX. The precipitates (PEGylated UCNPs@SiO_2-DOX) were dissolved in H_2O.

(6). PEGylated UCNPs@SiO_2-DOX Modification with Folic Acid (FA). The amino groups of FA were modified with carboxylate groups of PEG to form amide bonds through EDC/NHS chemistry. A solution of EDC (10 mM, 100 μL) and FA (2 mM, 100 μL) was mixed with PEGylated UCNPs@SiO_2-DOX at room temperature for 4 h. The collected precipitates by centrifugation of UNCP colloidal solutions were washed three times with DMSO to remove excess FA by centrifugation at 14 000 rpm for 30 min.

(7). Folate-PEGylated UCNPs@SiO_2-DOX Modification with Cage 2-Nitrobenzylamine Hydrochloride (NBA). The folate-PEGylated UCNPs@SiO_2-DOX particles (200 ppm), EDC (50 mM, 100 μL), and NBA (5 mM, 100 μL) were mixed for 2 days at room temperature. After 48 h, the particles were washed three times with deionized water by centrifugation at 15 000 rpm for 30 min. The caged folate-PEGylated UCNPs@SiO_2-DOX particles were dissolved in H_2O and was stable for 3 months.

Fluorescent Immunocytochemistry (ICC) Staining of Folate Receptor. HeLa (4×10^4/well), A549 (4×10^4/well), and MRC-5 (4×10^4/well) were seeded on Millicell EZ 4-well chamber slides (Millipore) and respective incubation with culture medium for 24 h. After the cells attached to the chamber slides, the cells were washed with PBS (phosphate buffered saline). Then cells were fixed for 20 min with 4% paraformaldehyde at room temperature, followed by addition of blocking buffer, and incubated for 45 min at room temperature. The negative control used the incubation buffer with no human FOLR1 (primary antibody) to characterize the nonspecific binding of antimouse IgG-NL493. Then the blocking buffer was removed, and diluted human FOLR1 (R&D MAB5646) was added with dilution buffer (ratio was 1:5) for incubating 3 h at room temperature, with added secondary antibodies

(NorthernLights antimouse IgG-NL493; R&D NL009; dilution 1:200) for another 1 h at room temperature. Then the slides were washed with PBS three times and mounting medium with DAPI added (VECTASHIELD) to cover coverslips. Fluorescence was observed using fluorescence microscopy (OLYMPUS, FLUOVIEW FV10i).

Phototargeting Evaluation of Caged Folate-PEGylated UCNPs@SiO_2 under Light Irradiation at 4 °C. HeLa (5×10^3) (or A549) cells/well were cultured in 96-well plates for 24 h, followed by treatment of 50 and 100 μg/mL (Y^{3+} concentration) of caged folate-PEGylated UCNPs@SiO_2 at 4 °C. Photolysis was performed using a 980 nm diode laser (11 W/cm^2) for 1 min irradiation, followed by additional 20 min incubation at 4 °C. Subsequently, the medium containing untargeted particles was removed by gentle rinsing of the cultures twice. Then, HNO_3/HCl mixture solution (volume ratio of HNO_3/HCl = 1/3) was added to lyse cells and UCNPs. The Y^{3+} ion concentrations were obtained by ICP-AES to determine the amount of UCNPs.

Cell Viability Evaluation of Free DOX, Folate-PEGylated UCNPs@SiO_2, Folate-PEGylated UCNPs@SiO_2-DOX, and Caged Folate-PEGylated UCNPs@SiO_2-DOX in the Absence of Light Irradiation. HeLa cells/well (5×10^3) were cultured in 96-well plates for 24 h, followed by treatment of 0, 5, 10, 50, and 100 μg/mL (Y^{3+} concentration) of folate-PEGylated UCNPs@SiO_2, folate-PEGylated UCNPs@SiO_2-DOX, and caged folate-PEGylated UCNPs@SiO_2-DOX, separately, at 4 °C for 20 min incubation. The 5, 10, 50, and 100 ppm correspond to 0.13, 0.27, 1.34, and 2.67 μM of DOX carried by the particles. The medium containing remaining materials was removed by gentle rinsing of the cultures twice, and then fresh medium was added. The subsequent 24 h incubation was conducted at 37 °C. The cell medium was replaced with fresh culture medium containing a 10% MTT reagent, and the cultures were incubated for 4 h to allow formazan dye to form. After removing the excess MTT medium, DMSO was added as a solvent. The DMSO solution in each well was centrifuged and collected and then transferred to an ELISA plate. The quantification of cell viability was done using an ELISA plate reader.

Cell Viability Evaluation of Caged Folate-PEGylated UCNPs@SiO_2-DOX under Light Irradiation. HeLa cells/well (5×10^3) were cultured in 96-well plates for 24 h, followed by treatment with 0, 5, 10, 50, and 100 μL of (Y^{3+} concentration) of caged folate-PEGylated UCNPs@SiO_2-DOX at 4 °C for exposure of a 980 nm diode laser for 1 or 2 min, followed by 20 min incubation at 4 °C. Subsequently, the medium containing untargeted particles was removed and fresh medium added. Then the additional culture at 37 °C for another 24 h was performed for particle internalization into cells.

After 24 h incubation, the medium containing remaining materials was removed by gentle rinsing of the cultures twice and fresh medium was added. The cell medium was replaced with fresh culture medium containing a 10% MTT reagent, and the cultures were incubated for 4 h to allow formazan dye to form. After excess MTT medium was removed, DMSO was added as a solvent. The DMSO solution in each well was centrifuged and collected and then transferred to an ELISA plate. The quantification of cell viability was done using an ELISA plate reader.

Cells Images of HeLa Cells Treated with UCNPs Using a Confocal Laser Scanning Microscope. Cells were cultured in α-modified MEM at 37 °C supplied with 5% CO_2/95% air. Cells were trypsinized and seeded in 8-well chamber slides with 1.2×10^4 cells in each well. After 24 h of incubation, each well was washed twice with phosphate buffered saline (PBS), and then 0.3 mL of caged folate-PEGylated UCNPs@SiO_2-DOX (100 μg/mL in α-modified DMEM) was added. The cells were then treated with UCNPs at 4 °C for exposure of a 980 nm diode laser for 2 min, followed by 20 min incubation at 4 °C. Then, the medium containing untargeted particles was removed and fresh medium added. Subsequently, the additional culture at 37 °C for 24 h was performed for particle internalization into cells. Then, the treated cells were washed with PBS and then fixed using 4% paraformaldehyde/PBS for 30 min at 37 °C. The cell cytoskeleton was stained with Alexa 488 phalloidin (green). The nuclei were stained with DAPI, and the cells treated with particles were subjected to a confocal laser scanning microscope (ECLIPSE Ti series, NIKON) equipped with NIR 980 nm diode laser for observation.

Fluorescent Immunocytochemistry (ICC) Staining of LysoTracker Green. HeLa (2×10^4/well) cells were seeded on NUNC Lab-Tek 4-well chamber slides and incubated with respective culture medium for 24 h. After the cells had attached to the chamber slides, the cells were washed with 1× PBS. Folate-PEGylated UCNP@SiO_2-DOX and caged folate-PEGylated UCNP@SiO_2-DOX in 1× PBS (dosage: 50 ppm of [Y^{3+}]) were added individually and incubated at 4 °C for 20 min, and then the cells were washed with 1× PBS. Free FBS medium was added to the cells, and cells were incubated for an additional 24 h at 37 °C. Medium was removed from the dish and added to the prewarmed probe-containing medium (Invitrogen; L7526). Then, the cells were incubated at 37 °C for 2 h. After replacing the loading solution with free FBS medium, the cells were subjected to observation using a fluorescence microscope (OLYMPUS, FLUOVIEW FV1000). The ex/em of DOX was 565/665, and LysoTracker was 490/555.

Tumor-Bearing Animal Models and Tumor Size Monitoring. The animal study protocol was approved by Chang Gung Memorial Hospital Laboratory Animal Center (Kaohsiung, Taiwan). To assess tumorigenicity, nude mice NU/NU (6−8 weeks old and 25−30 g weight) were purchased from Chang Gung Memorial Hospital Laboratory Animal Center. HeLa cells were grown to 80% confluence and then harvested and resuspended in PBS. Mouse tumor xenografts were established by subdermal region injection of HeLa cells with 6×10^6 cells per flank. After 8 days of tumor xenografts, the tumor-bearing mice were ready for studies.

To evaluate the efficacy of caged folate-PEGylated UCNPs@SiO_2-DOX in anticancer therapy, we used 30 tumor-bearing mice that were divided into six groups including control (PBS received), free DOX, laser only, caged folate-PEGylated UCNPs@SiO_2-DOX, PEGylated UCNPs@SiO_2-DOX + laser, and caged folate-PEGylated UCNPs@SiO_2-DOX + laser. The tumor size was calculated using the following formula: [(large diameter) × (small diameter)^2]/2. The mice with the tumors (~92 mm^3) were injected with caged folate-PEGylated UCNPs@SiO_2-DOX with a dosage of 2 mg DOX/kg through the tail vein. Tumors were exposed to 980 nm (1.8 W/cm^2) laser irradiation of 1 h after particles were injected into mice for the group of PEGylated UCNPs@SiO_2-DOX + laser and caged folate-PEGylated UCNPs@SiO_2-DOX + laser. The group with laser only received exposure of irradiation for 1 h. The group treated with free DOX received intravenous injection using the same amount of DOX carried by UNCPs.

***In Vivo* and *Ex Vivo* Imaging Assessments of Caged Folate-PEGylated UCNPs@SiO_2-DOX Nanoparticles in Tumor-Bearing Mice.** The whole body tumor-bearing mice were imaged at preinjection, post-1, 3, 5, and 24 h (n = 5 each). Caged folate-PEGylated UCNPs@SiO_2-DOX nanoparticles (at a dose of 2 mg DOX/kg) were administered to the mice through tail vein injection. For *ex vivo* imaging, the mice were sacrificed at post-1, 5, and 24 h, and the vital organs were isolated for optical imaging. Real-time fluorescent imaging was monitored using IVIS Spectrum with a cooled CCD optical system equipped with fluorescent filter sets (excitation/emission = 980/800 nm for the upconversion NIR emission of caged folate-PEGylated UCNPs@SiO_2-DOX; excitation/emission = 500/580 nm for *ex vivo* DOX images). Prior to imaging, tumor-bearing mice were anesthetized with 2% isofluorane. The field of view was 125 mm in diameter. The images were acquired for 0.5 s using Living Image Analysis and acquisition software. A photographic image was taken, onto which the pseudocolor image representing the spatial distribution of photon counts was projected.

Conflict of Interest: The authors declare no competing financial interest.

Acknowledgment. This work was supported by the National Science Council (NSC101-2113-M-006-004-MY2) of Taiwan, and Kaohsiung Chang Gung Memorial Hospital, Taiwan (CMRPG8A1022).

Supporting Information Available: TEM, UV−vis, FTIR spectra, HPLC spectra, NMR spectra, and the fluorescent immunocytochemistry staining of folate-PEGylated UCNPs@SiO_2 and caged folate-PEGylated UCNPs@SiO_2-DOX. This material is available free of charge *via* the Internet at http://pubs.acs.org.

REFERENCES AND NOTES

1. Dvir, T.; Banghart, M. R.; Timko, B. P.; Langer, R.; Kohane, D. S. Photo-targeted Nanoparticles. *Nano Lett.* **2010**, *10*, 250–254.
2. Shamay, Y.; Adar, L.; Ashkenasy, G.; David, A. Light Induced Drug Delivery into Cancer Cells. *Biomaterials* **2011**, *32*, 1377–1386.
3. Fan, N. C.; Cheng, F. Y.; Ho, J. A.; Yeh, C. S. Photocontrolled Targeted Drug Delivery: Photocaged Biologically Active Folic Acid as a Light-Responsive Tumor-Targeting Molecule. *Angew. Chem., Int. Ed.* **2012**, *51*, 8806–8810.
4. Li, Z.; Zhang, Y. Monodisperse Silica-Coated Polyvinylpyrrolidone/$NaYF_4$ Nanocrystals with Multicolor Upconversion Fluorescence Emission. *Angew. Chem., Int. Ed.* **2006**, *45*, 7732–7735.
5. Wang, F.; Liu, X. Upconversion Multicolor Fine-Tuning: Visible to Near-Infrared Emission from Lanthanide-Doped $NaYF_4$ Nanoparticles. *J. Am. Chem. Soc.* **2008**, *130*, 5642–5643.
6. Abel, K. A.; Boyer, J. C.; van Veggel, F. C. Hard Proof of the $NaYF_4$/$NaGdF_4$ Nanocrystal Core/Shell Structure. *J. Am. Chem. Soc.* **2009**, *131*, 14644–14645.
7. Wang, F.; Han, Y.; Lim, C. S.; Lu, Y.; Wang, J.; Xu, J.; Chen, H.; Zhang, C.; Hong, M.; Liu, X. Simultaneous Phase and Size Control of Upconversion Nanocrystals through Lanthanide Doping. *Nature* **2010**, *463*, 1061–1065.
8. Wang, F.; Wang, J.; Liu, X. Direct Evidence of a Surface Quenching Effect on Size-Dependent Luminescence of Upconversion Nanoparticles. *Angew. Chem., Int. Ed.* **2010**, *49*, 7456–7460.
9. Carling, C. J.; Nourmohammadian, F.; Boyer, J. C.; Branda, N. R. Remote-Control Photorelease of Caged Compounds Using Near-Infrared Light and Upconverting Nanoparticles. *Angew. Chem., Int. Ed.* **2010**, *49*, 3782–3785.
10. Bogdan, N.; Vetrone, F.; Ozin, G. A.; Capobianco, J. A. Synthesis of Ligand-Free Colloidally Stable Water Dispersible Brightly Luminescent Lanthanide-Doped Upconverting Nanoparticles. *Nano Lett.* **2011**, *11*, 835–840.
11. Haase, M.; Schafer, H. Upconverting Nanoparticles. *Angew. Chem., Int. Ed.* **2011**, *50*, 5808–5829.
12. Wang, J.; Wang, F.; Wang, C.; Liu, Z.; Liu, X. Single-Band Upconversion Emission in Lanthanide-Doped $KMnF_3$ Nanocrystals. *Angew. Chem., Int. Ed.* **2011**, *50*, 10369–10372.
13. Tu, D.; Liu, L.; Ju, Q.; Liu, Y.; Zhu, H.; Li, R.; Chen, X. Time-Resolved FRET Biosensor Based on Amine-Functionalized Lanthanide-Doped $NaYF_4$ Nanocrystals. *Angew. Chem., Int. Ed.* **2011**, *50*, 6306–6310.
14. Wu, S.; Han, G.; Milliron, D. J.; Aloni, S.; Altoe, V.; Talapin, D. V.; Cohen, B. E.; Schuck, P. J. Non-blinking and Photostable Upconverted Luminescence from Single Lanthanide-Doped Nanocrystals. *Proc. Natl. Acad. Sci. U.S.A.* **2009**, *106*, 10917–10921.
15. Yong Il, P.; Jeong Hyun, K.; Kang Taek, L.; Ki-Seok, J.; Hyon Bin, N.; Jung Ho, Y.; Hyung Min, K.; Nohyun, L.; Seung Hong, C.; Sung-Il, B.; *et al.* Nonblinking and Nonbleaching Upconverting Nanoparticles as an Optical Imaging Nanoprobe and T_1 Magnetic Resonance Imaging Contrast Agent. *Adv. Mater.* **2009**, *21*, 4476–4471.
16. Nam, S. H.; Bae, Y. M.; Park, Y. I.; Kim, J. H.; Kim, H. M.; Choi, J. S.; Lee, K. T.; Hyeon, T.; Suh, Y. D. Long-Term Real-Time Tracking of Lanthanide Ion Doped Upconverting Nanoparticles in Living Cells. *Angew. Chem., Int. Ed.* **2011**, *50*, 6093–6097.
17. Chen, Z.; Chen, H.; Hu, H.; Yu, M.; Li, F.; Zhang, Q.; Zhou, Z.; Yi, T.; Huang, C. Versatile Synthesis Strategy for Carboxylic Acid-Functionalized Upconverting Nanophosphors as Biological Labels. *J. Am. Chem. Soc.* **2008**, *130*, 3023–3029.
18. Nyk, M.; Kumar, R.; Ohulchanskyy, T. Y.; Bergey, E. J.; Prasad, P. N. High Contrast *In Vitro* and *In Vivo* Photoluminescence Bioimaging Using Near-Infrared to Near-Infrared Upconversion in Tm^{3+} and Yb^{3+} Doped Fluoride Nanophosphors. *Nano Lett.* **2008**, *8*, 3834–3838.
19. Chatterjee, D. K.; Rufaihah, A. J.; Zhang, Y. Upconversion Fluorescence Imaging of Cells and Small Animals Using Lanthanide Doped Nanocrystals. *Biomaterials* **2008**, *29*, 937–943.
20. Xiong, L. Q.; Chen, Z. G.; Yu, M. X.; Li, F. Y.; Liu, C.; Huang, C. H. Synthesis, Characterization, and *In Vivo* Targeted Imaging of Amine-Functionalized Rare-Earth Up-converting Nanophosphors. *Biomaterials* **2009**, *30*, 5592–5600.
21. Xiong, L.; Yang, T.; Yang, Y.; Xu, C.; Li, F. Long-Term *In Vivo* Biodistribution Imaging and Toxicity of Polyacrylic Acid-Coated Upconversion Nanophosphors. *Biomaterials* **2010**, *31*, 7078–7085.
22. Liu, J.; Liu, Y.; Liu, Q.; Li, C.; Sun, L.; Li, F. Iridium(III) Complex-Coated Nanosystem for Ratiometric Upconversion Luminescence Bioimaging of Cyanide Anions. *J. Am. Chem. Soc.* **2011**, *133*, 15276–15279.
23. Deng, R.; Xie, X.; Vendrell, M.; Chang, Y. T.; Liu, X. Intracellular Glutathione Detection Using MnO_2-Nanosheet-Modified Upconversion Nanoparticles. *J. Am. Chem. Soc.* **2011**, *133*, 20168–20171.
24. Xia, A.; Gao, Y.; Zhou, J.; Li, C.; Yang, T.; Wu, D.; Wu, L.; Li, F. Core–Shell $NaYF_4$:Yb^{3+},Tm^{3+}@Fe_xO_y Nanocrystals for Dual-Modality T_2-Enhanced Magnetic Resonance and NIR-to-NIR Upconversion Luminescent Imaging of Small-Animal Lymphatic Node. *Biomaterials* **2011**, *32*, 7200–7208.
25. Yang, Y.; Shao, Q.; Deng, R.; Wang, C.; Teng, X.; Cheng, K.; Cheng, Z.; Huang, L.; Liu, Z.; Liu, X.; *et al.* *In Vitro* and *In Vivo* Uncaging and Bioluminescence Imaging by Using Photocaged Upconversion Nanoparticles. *Angew. Chem., Int. Ed.* **2012**, *51*, 3125–3129.
26. Li, L. L.; Zhang, R.; Yin, L.; Zheng, K.; Qin, W.; Selvin, P. R.; Lu, Y. Biomimetic Surface Engineering of Lanthanide-Doped Upconversion Nanoparticles as Versatile Bioprobes. *Angew. Chem., Int. Ed.* **2012**, *51*, 6121–6125.
27. Ju, Q.; Tu, D.; Liu, Y.; Li, R.; Zhu, H.; Chen, J.; Chen, Z.; Huang, M.; Chen, X. Amine-Functionalized Lanthanide-Doped $KGdF_4$ Nanocrystals as Potential Optical/Magnetic Multimodal Bioprobes. *J. Am. Chem. Soc.* **2012**, *134*, 1323–1330.
28. Hou, Y.; Qiao, R.; Fang, F.; Wang, X.; Dong, C.; Liu, K.; Liu, C.; Liu, Z.; Lei, H.; Wang, F.; *et al.* $NaGdF_4$ Nanoparticle-Based Molecular Probes for Magnetic Resonance Imaging of Intraperitoneal Tumor Xenografts *in Vivo*. *ACS Nano* **2013**, *7*, 330–338.
29. Wang, C.; Tao, H.; Cheng, L.; Liu, Z. Near-Infrared Light Induced *In Vivo* Photodynamic Therapy of Cancer Based on Upconversion Nanoparticles. *Biomaterials* **2011**, *32*, 6145–6154.
30. Idris, N. M.; Gnanasammandhan, M. K.; Zhang, J.; Ho, P. C.; Mahendran, R.; Zhang, Y. *In Vivo* Photodynamic Therapy Using Upconversion Nanoparticles as Remote-Controlled Nanotransducers. *Nat. Med.* **2012**, *18*, 1580–1585.
31. Park, Y. I.; Kim, H. M.; Kim, J. H.; Moon, K. C.; Yoo, B.; Lee, K. T.; Lee, N.; Choi, Y.; Park, W.; Ling, D.; *et al.* Theranostic Probe Based on Lanthanide-Doped Nanoparticles for Simultaneous *In Vivo* Dual-Modal Imaging and Photodynamic Therapy. *Adv. Mater.* **2012**, *24*, 5755–5761.
32. Sisi, C.; Haiyan, C.; Hongyan, Z.; Junmei, T.; Xuemei, C.; Zhiyu, Q.; Samuel, A.; Yueqing, G. Amphiphilic Chitosan Modified Upconversion Nanoparticles for *In Vivo* Photodynamic Therapy Induced by Near-Infrared Light. *J. Mater. Chem.* **2012**, *22*, 4861–4873.
33. Cui, S.; Yin, D.; Chen, Y.; Di, Y.; Chen, H.; Ma, Y.; Achilefu, S.; Gu, Y. *In Vivo* Targeted Deep-Tissue Photodynamic Therapy Based on Near-Infrared Light Triggered Upconversion Nanoconstruct. *ACS Nano* **2013**, *7*, 676–688.
34. Chao, W.; Liang, C.; Yumeng, L.; Xiaojing, W.; Xinxing, M.; Zhaoyi, D.; Yonggang, L.; Zhuang, L. Imaging-Guided pH-Sensitive Photodynamic Therapy Using Charge Reversible Upconversion Nanoparticles under Near-Infrared Light. *Adv. Funct. Mater.* **2013**, *23*, 3077–3086.
35. Wang, C.; Cheng, L.; Liu, Z. Drug Delivery with Upconversion Nanoparticles for Multi-functional Targeted Cancer Cell Imaging and Therapy. *Biomaterials* **2011**, *32*, 1110–1120.
36. Xu, Z.; Ma, P. A.; Li, C.; Hou, Z.; Zhai, X.; Huang, S.; Lin, J. Monodisperse Core–Shell Structured Up-Conversion

$Yb(OH)CO_3$@$YbPO_4$:Er^{3+} Hollow Spheres as Drug Carriers. *Biomaterials* **2011**, *32*, 4161–4173.

37. Tian, G.; Gu, Z.; Zhou, L.; Yin, W.; Liu, X.; Yan, L.; Jin, S.; Ren, W.; Xing, G.; Li, S.; *et al.* Mn^{2+} Dopant-Controlled Synthesis of $NaYF_4$:Yb/Er Upconversion Nanoparticles for *In Vivo* Imaging and Drug Delivery. *Adv. Mater.* **2012**, *24*, 1226–1231.
38. Xu, Z.; Li, C.; Ma, P.; Hou, Z.; Yang, D.; Kang, X.; Lin, J. Facile Synthesis of an Up-Conversion Luminescent and Mesoporous Gd_2O_3:Er^{3+}@*n*SiO_2@*m*SiO_2 Nanocomposite as a Drug Carrier. *Nanoscale* **2011**, *3*, 661–667.
39. Sudimack, J.; Lee, R. J. Targeted Drug Delivery *via* the Folate Receptor. *Adv. Drug Delivery Rev.* **2000**, *41*, 147–162.
40. Kamen, B. A.; Smith, A. K. A Review of Folate Receptor Alpha Cycling and 5-Methyltetrahydrofolate Accumulation with an Emphasis on Cell Models *in Vitro*. *Adv. Drug Delivery Rev.* **2004**, *56*, 1085–1097.
41. Hilgenbrink, A. R.; Low, P. S. Folate Receptor-Mediated Drug Targeting: From Therapeutics to Diagnostics. *J. Pharm. Sci.* **2005**, *94*, 2135–2146.
42. Ross, J. F.; Chaudhuri, P. K.; Ratnam, M. Differential Regulation of Folate Receptor Isoforms in Normal and Malignant Tissues *in Vivo* and in Established Cell Lines. Physiologic and Clinical Implications. *Cancer* **1994**, *73*, 2432–2443.
43. Elnakat, H.; Ratnam, M. Distribution, Functionality and Gene Regulation of Folate Receptor Isoforms: Implications in Targeted Therapy. *Adv. Drug Delivery Rev.* **2004**, *56*, 1067–1084.
44. Weitman, S. D.; Lark, R. H.; Coney, L. R.; Fort, D. W.; Frasca, V.; Zurawski, V. R., Jr.; Kamen, B. A. Distribution of the Folate Receptor GP38 in Normal and Malignant Cell Lines and Tissues. *Cancer Res.* **1992**, *52*, 3396–3401.
45. Xia, W.; Low, P. S. Folate-Targeted Therapies for Cancer. *J. Med. Chem.* **2010**, *53*, 6811–6824.
46. Muller, C.; Forrer, F.; Schibli, R.; Krenning, E. P.; de Jong, M. SPECT Study of Folate Receptor-Positive Malignant and Normal Tissues in Mice Using a Novel 99mTc-Radiofolate. *J. Nucl. Med.* **2008**, *49*, 310–317.
47. Derfus, A. M.; Chen, A. A.; Min, D. H.; Ruoslahti, E.; Bhatia, S. N. Targeted Quantum Dot Conjugates for siRNA Delivery. *Bioconjugate Chem.* **2007**, *18*, 1391–1396.
48. Ishida, T.; Kirchmeier, M. J.; Moase, E. H.; Zalipsky, S.; Allen, T. M. Targeted Delivery and Triggered Release of Liposomal Doxorubicin Enhances Cytotoxicity Against Human B Lymphoma Cells. *Biochim. Biophys. Acta* **2001**, *1515*, 144–158.
49. Kirpotin, D.; Hong, K.; Mullah, N.; Papahadjopoulos, D.; Zalipsky, S. Liposomes with Detachable Polymer Coating: Destabilization and Fusion of Dioleoylphosphatidylethanolamine Vesicles Triggered by Cleavage of Surface-Grafted Poly(ethylene glycol). *FEBS Lett.* **1996**, *388*, 115–118.
50. Zalipsky, S.; Qazen, M.; Walker, J. A., II; Mullah, N.; Quinn, Y. P.; Huang, S. K. New Detachable Poly(ethylene glycol) Conjugates: Cysteine-Cleavable Lipopolymers Regenerating Natural Phospholipid, Diacyl Phosphatidylethanolamine. *Bioconjugate Chem.* **1999**, *10*, 703–707.
51. Li, Z.; Zhang, Y. An Efficient and User-Friendly Method for the Synthesis of Hexagonal-Phase $NaYF_4$:Yb,Er/Tm Nanocrystals with Controllable Shape and Upconversion Fluorescence. *Nanotechnology* **2008**, *19*, 345606–345610.
52. Li, Z. Q.; Zhang, Y.; Jiang, S. Multicolor Core/Shell-Structured Upconversion Fluorescent Nanoparticles. *Adv. Mater.* **2008**, *20*, 4765–4769.
53. Wang, G.; Qin, W.; Wang, L.; Wei, G.; Zhu, P.; Kim, R. Intense Ultraviolet Upconversion Luminescence from Hexagonal $NaYF_4$:Yb^{3+}/Tm^{3+} Microcrystals. *Opt. Express* **2008**, *16*, 11907–11914.
54. Wang, F.; Deng, R.; Wang, J.; Wang, Q.; Han, Y.; Zhu, H.; Chen, X.; Liu, X. Tuning Upconversion through Energy Migration in Core−Shell Nanoparticles. *Nat. Mater.* **2011**, *10*, 968–973.
55. Graf, C.; Vossen, D. L. J.; Imhof, A.; van Blaaderen, A. A General Method To Coat Colloidal Particles with Silica. *Langmuir* **2003**, *19*, 6693–6700.
56. Yi, G.; Lu, H.; Zhao, S.; Ge, Y.; Yang, W.; Chen, D.; Guo, L.-H. Synthesis, Characterization, and Biological Application of Size-Controlled Nanocrystalline $NaYF_4$:Yb,Er Infrared-to-Visible Up-Conversion Phosphors. *Nano Lett.* **2004**, *4*, 2191–2196.
57. Zhang, P.; Rogelj, S.; Nguyen, K.; Wheeler, D. Design of a Highly Sensitive and Specific Nucleotide Sensor Based on Photon Upconverting Particles. *J. Am. Chem. Soc.* **2006**, *128*, 12410–12411.
58. Liu, L.; Li, B.; Qin, R.; Zhao, H.; Ren, X.; Su, Z. Synthesis and Characterization of Nanoporous $NaYF_4$:Yb^{3+},Tm^{3+}@SiO_2 Nanocomposites. *Solid State Sci.* **2010**, *12*, 345–349.
59. Greenfield, R. S.; Kaneko, T.; Daues, A.; Edson, M. A.; Fitzgerald, K. A.; Olech, L. J.; Grattan, J. A.; Spitalny, G. L.; Braslawsky, G. R. Evaluation *In Vitro* of Adriamycin Immunoconjugates Synthesized Using an Acid-Sensitive Hydrazone Linker. *Cancer Res.* **1990**, *50*, 6600–6607.
60. Wang, S.; Lee, R. J.; Mathias, C. J.; Green, M. A.; Low, P. S. Synthesis, Purification, and Tumor Cell Uptake of 67Ga-Deferoxamine—Folate, a Potential Radiopharmaceutical for Tumor Imaging. *Bioconjugate Chem.* **1996**, *7*, 56–62.
61. Blitzer, J. T.; Nusse, R. A Critical Role for Endocytosis in WNT Signaling. *BMC Cell Biol.* **2006**, *7*, 28–39.
62. Khalil, I. A.; Kogure, K.; Akita, H.; Harashima, H. Uptake Pathways and Subsequent Intracellular Trafficking in Nonviral Gene Delivery. *Pharmacol. Rev.* **2006**, *58*, 32–45.
63. Hergt, R.; Dutz, S.; Muller, R.; Zeisberger, M. Magnetic Particle Hyperthermia: Nanoparticle Magnetism and Materials Development for Cancer Therapy. *J. Phys.: Condens. Matter* **2006**, *18*, S2919–S2934.
64. Gormley, A. J.; Larson, N.; Sadekar, S.; Robinson, R.; Ray, A.; Ghandehari, H. Guided Delivery of Polymer Therapeutics Using Plasmonic Phtothermal Therapy. *Nano Today* **2012**, *7*, 158–167.